

pubs.acs.org/jcim Article

Transmembrane β -Barrel Models of α -Synuclein Oligomers

Manuela Maurer and Themis Lazaridis*



Cite This: J. Chem. Inf. Model. 2023, 63, 7171-7179



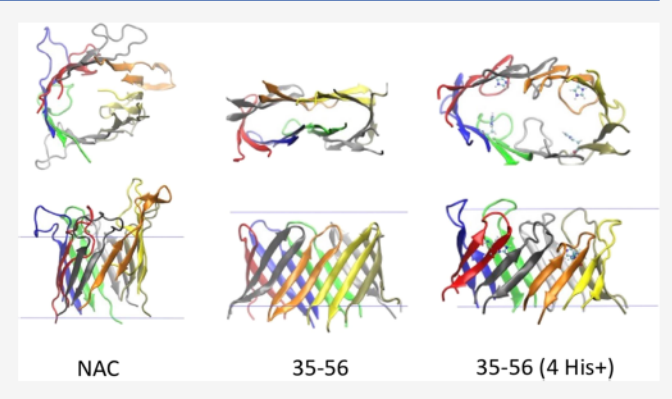
ACCESS

Metrics & More

Article Recommendations

Supporting Information

ABSTRACT: The aggregation of α -synuclein is implicated in a number of neurodegenerative diseases, such as Parkinson's and Multiple System Atrophy, but the role of these aggregates in disease development is not clear. One possible mechanism of cytotoxicity is the disturbance or permeabilization of cell membranes by certain types of oligomers. However, no high-resolution structure of such membrane-embedded complexes has ever been determined. Here we construct and evaluate putative transmembrane β -barrels formed by this protein. Examination of the α -synuclein sequence reveals two regions that could form membrane-embedded β -hairpins: 64–92 (the NAC), and 35–56, which harbors many familial Parkinson's mutations. The stability of β -barrels formed by these hairpins is examined first in implicit



membrane pores and then by multimicrosecond all-atom simulations. We find that a NAC region barrel remains stably inserted and hydrated for at least 10 μ s. A 35–56 barrel remains stably inserted in the membrane but dehydrates and collapses if all His50 are neutral or if His50 is replaced by Q. If half of the His50 are doubly protonated, the barrel takes an oval shape but remains hydrated for at least 10 μ s. Possible implications of these findings for α -synuclein pathology are discussed.

■ INTRODUCTION

α-synuclein (aS) is a 140-residue protein implicated in several neurodegenerative diseases. It is the major component of the intracellular Lewy bodies observed in Parkinson's and in Dementia with Lewy Bodies¹ and of cytoplasmic inclusions observed in Multiple System Atrophy.² Its physiological function is poorly understood.^{3,4} In solution and in cells aS is largely unfolded,^{5,6} but interaction with lipids shifts the N-terminal domain (res. 1–95) into a helical conformation, which can be broken in micelles^{7–9} or extended on vesicles^{10–12} or sampling both conformations.¹³ In vitro, aS aggregates into fibrils of varying structures.^{14–18} Fragment microcrystals have also been determined in which residues 69–78 make parallel β-sheets.¹⁹ In addition to fibrils, aS forms a variety of soluble oligomers.²⁰ The structure of these oligomers is largely unknown, although some low-resolution information has been gleaned from various biophysical methods.^{21–24}

As with other amyloidogenic proteins, toxicity seems to be highest for αS oligomers, $^{25,26}_{-27,28}$ although some reports find fibrils to be the toxic species. 27,28 Various mechanisms of toxicity have been considered. 29 Prominent among them is membrane permeabilization. $^{26,30-41}$ Many studies found no permeabilization by monomeric αS . 30,39,40 Others reported leakage from liposomes caused by unincubated (presumably monomeric) αS , but usually at higher concentrations, 42,43 or voltage-induced ion channels under conditions where the protein is a long helix on the membrane surface. 37 Solid state NMR showed that in the toxic oligomers residues 70–88 had β

structure and inserted in the membrane, while the N-terminus was dynamic and accessible, with the first 25 residues binding to the membrane.³³

Most theoretical studies on aS have been concerned with aggregation in solution⁴⁴ and only a few with its interaction with membranes.^{45–47} Some models of membrane-inserted pore-forming complexes have been proposed, both helical^{48,49} and β -sheet,⁵⁰ but have not been tested and are difficult to replicate and evaluate due to the unavailability of coordinates. Some time ago our lab examined the binding of the N-terminal helix on an implicit membrane⁵¹ and more recently the dependence of this binding on membrane curvature.⁵² Here we consider the hypothesis that aggregated aS makes β -barrel supported pores in membranes. We build putative models of these pores, examine their stability using implicit and explicit-solvent simulations, and discuss their plausibility in light of the available experimental data.

Received: July 3, 2023
Revised: October 20, 2023
Accepted: October 25, 2023
Published: November 14, 2023





Table 1

MDVFMKGLSK	AKEG VV AAAE	KTKQG $oldsymbol{V}$ AEAA	GKTKEGVLYV	GSKTKEG VV H	50
$G\mathbf{V}$ AT \mathbf{V} AEK \mathbf{T} K	${ t E}{ t Q}{f V}{ t T}{ t N}{f V}{ t G}{ t G}{ t A}{f V}$	\mathbf{V} TG \mathbf{V} TA \mathbf{V} AQK	TVEGAGSIAA	$\mathtt{ATG}\mathbf{FV}\mathtt{KKDQL}$	100
GKNEEGAPQE	GILEDMPVDP	DNEA Y E M PSE	EG Y QD Y EPEA		140

RESULTS

Model Construction and Implicit Solvent Modeling. The sequence of aS is displayed in Table 1 (strongly hydrophobic residues are shown in bold).

Examination of transmembrane β -barrel structures reveals that each β -strand typically exposes five side chains to the membrane, and one of them is often Gly. 53,54 Two side chains are near the hydrophobic-hydrophilic interface and three are deeply in the hydrophobic core. Thus, we looked for stretches containing triplets of nonpolar residues separated by one residue (i.e., $\Phi \times \Phi \times \Phi$, where Φ is a hydrophobe). One of them need not be strongly hydrophobic (e.g., A or G) but it cannot be strongly polar. The 40-residue C-terminal domain is disordered and rich in acidic residues. In addition, it lacks a Φ $\times \Phi \times \Phi$ motif and is thus unlikely to insert into the membrane. Residues 61-95 comprise the so-called NAC (Non-Amyloid β Component of Alzheimer's plaques), and are most prone to aggregation. The NAC is the most obvious candidate for membrane insertion. Another stretch that contains sufficient numbers of hydrophobic residues is 35-56. We focused on these two regions and explored the possibility of insertion of β -hairpins.

We considered octamers of hairpins because they create pores sufficiently large for ion conduction. We used our previous β -barrel of eight protegrin β -hairpins⁵⁵ as a template and considered different alignments for the NAC (Table 2).

Table 2. Possible Alignments of the NAC Region with the Protegrin Hairpin and Their Transfer Energy from Water to the $Pore^a$

		ΔW (kcal/mol)
1.	RGGRLCYCRRRFCVCVGR	
	70-VTGVTAVAQKTVEGAGSI-88	+3
2.	rg g r l c y cr rr f c v c v gr	
	68-GA V V T G V TA V AQKT V E G A G S I AAA-91	0
3.	RGGRLCYCR RRFCVCVGR	
6	1-EQVTN V G G A V VTGVTAVAQKT V E G A G S I AAATGFV	+5
4.	RGGRLCYCR RRFCVCVGR	
	EQVTN V GGA V VTGVTAVAQKT V EGAGSIAAATGFV	-13
5.	RGGRLCYCR RRFCVCVGR	
	EQVTN V G G A V VTGVTAVAQKT V E G A G S I A A A T GFV	-15
6.	rg g r l c y cr rr f c v c v gr	
	68-GA V V T G V TA V AQKT V E G A G S I AAA-91	+6
7.	RGGRLCYCRRRFCVCVGR	
	EQV-TNVGGAVVT GVTAVAQK-TVEGAGSIAAATGFV	-6
8.	RGGRLCYCRRRFCVCVGR	
	EQV-TNVGGAVVT GVTAVAQK-TVEGAGSIAAATGFV	-3

^aThe first line in each alignment is the protegrin sequence. In bold are the residues facing lipids.

The stability of the model was judged by (a) how well preserved the barrel structure was, (b) whether it stayed in the pore, and (c) the magnitude of the transfer energy ΔW from water to the pore. Some alignments (e.g., #4) showed a favorable ΔW but the barrel either broke or moved partly out of the pore. Other alignments preserved the structure of the barrel but exhibited an unfavorable transfer energy. The best overall was alignment #5 with favorable ΔW and a reasonable barrel structure (Figure 1). This model was selected for further study using all-atom simulations.

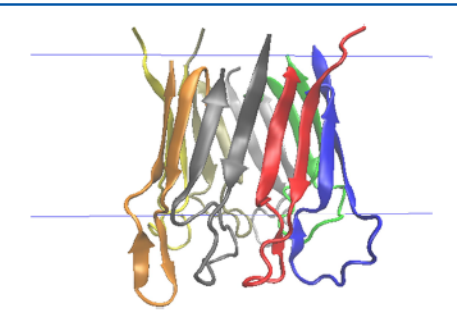
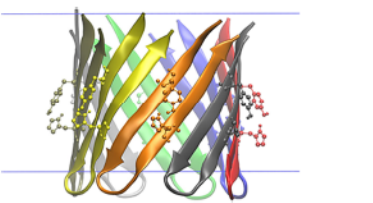


Figure 1. NAC barrel alignment 5. Blue lines indicate the implicit membrane-water interface.

Section 35–56 also has enough hydrophobic residues to possibly insert into the membrane. Two models were constructed based on the NMR structure of this fragment in complex with a protein engineered to bind it (pdb id 4BXL). The two models differ in which side of the hairpin faces inside/out. In 4BXL one face of the hairpin has the side chains of residues V37, Y39, G41, V48, H50, V52, T54, A56 and the other L38, V40, S42, V49, G51, A53, V55. The hydrophobicity of the latter face seems higher than that of the former. Indeed, the model with Y39 and H50 pointing inside (Figure 2)



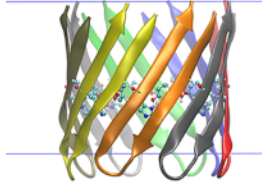


Figure 2. Initial 35–56 barrel models based on 4BXL. Left: Y39 and H50 facing outward. Right: Y39 and H50 facing inward. The latter model was chosen for further study. Blue lines indicate the implicit membrane - water interface.

Table 3. Barrel Models for Fragment 35-56 of aS^a

1. 4BXL-based octamer,	(V II)	ΔW (kcal/mol)	
EGVLYVGSKTKEGVVHGVATVA	(YinHin)	-25	
2. 4BXL-based octamer, EG V L Y V G SKTKEG V V H G V ATVA	(Y _{out} H _{out})	+27	
3. RGGRLCYCR_RRFCVCVGR, GVLYVGSKTKEGVVHGVAT	$(Y_{in}H_{out})$	-14	

^aIn bold are side chains facing outwards.

exhibited favorable insertion energy (Table 3), so it was selected for further study by all-atom MD. It is possible to construct models with one strand flipped. For example, model 3 based on our protegrin octamer has the C-terminal strand flipped compared to model 1 and exhibits favorable insertion energy, albeit less than $Y_{\rm in}H_{\rm in}$.

All-Atom Simulations. NAC Barrel. The 64–92 model (NACS) remains stable with limited structural changes during

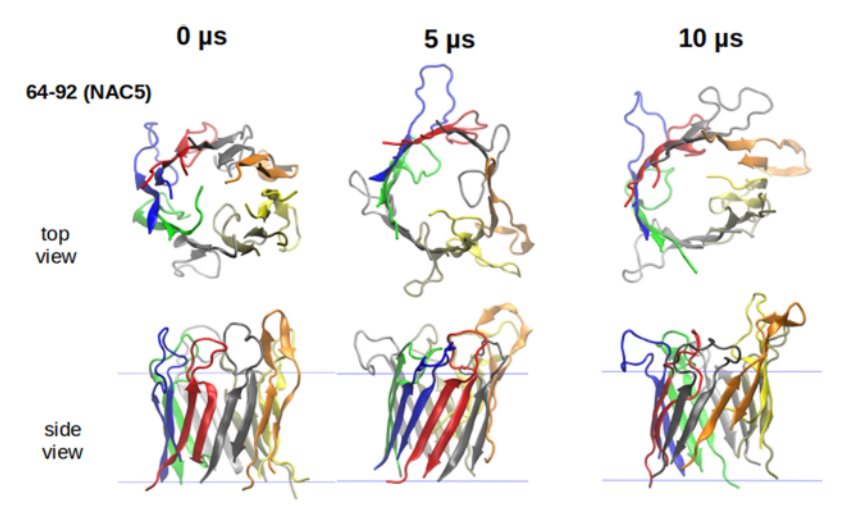


Figure 3. NAC5 barrel at 0, 5, and 10 μ s of all-atom simulation.

the 10 μ s all-atom simulation. Initial, middle, and final structures are shown in Figure 3. The N-terminus of hairpin E (yellow) is more mobile than the others and often forms salt bridges to the C-terminus of hairpin G (light gray), or to glutamic acid side chains. Between 1.6 and 2.5 μ s hairpin E imparts much disorder unto hairpin D (orange). During this time, the H-bond register within hairpin D changes from GLY5:O-ALA27:N initially to GLY5:O-THR29:N. The H-bond register between hairpins C and D also shifts by one from (C)SER24:O-(D)VAL8:N to (C)SER24:O-(D)ALA6:N. The increased shear causes the C-terminal strand of D and the N-terminal strand of E to slide deeper into the aqueous phase, but their β -sheet content remains relatively constant, as shown in Figure 4. The total β -sheet content oscillates around 37% up to

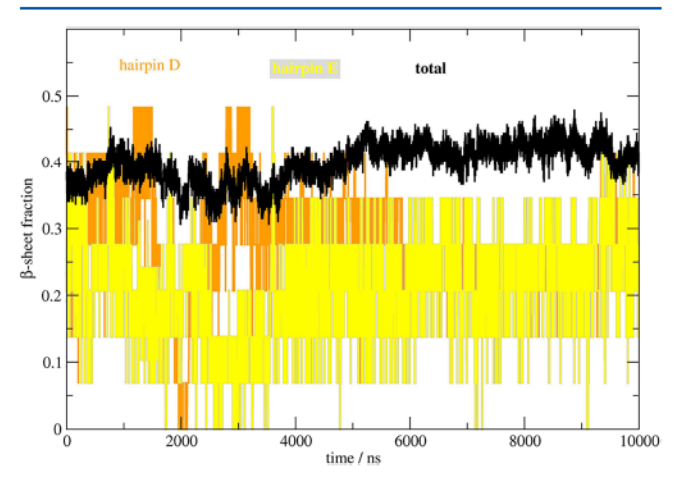


Figure 4. β -sheet content in the NAC5 during 10 μ s. Black line is for the entire complex and colored lines for hairpins D and E.

4 μ s, then increases slightly to 42%. The barrel's overall shape also visually seems to improve at that point. It then remains open and hydrated in this state for the remaining 6 μ s. RMSD and radius of gyration plots for this and the other all-atom simulations are shown in Figures S1 and S2 in SI, respectively. A plot of the number of water molecules in the NAC5 barrel is shown in Figure S3 in SI.

35–56 Barrel. During the first 5 μ s, the 35–56 $Y_{in}H_{in}$ barrel gradually flattens (Figure 5), although the β -strands themselves remain relatively ordered and the total β -sheet content remains

stable at about 60% throughout. The final structure's interior is mostly dry. Figure 6 shows the number of water molecules within the barrel diminishing over time. This is clearly due to the predominantly hydrophobic nature of the barrel interior. The only polar residues are Y39 and H50. The (partially polar) Y39 residues mainly point toward the termini and the H50 residues toward the loops; they H-bond with each other when opposite strands come close after the barrel's collapse. The $Y_{out}H_{out}$ model has an even more hydrophobic interior and already flattened during equilibration in implicit solvent (Figure S4).

H50Q is a familial mutation in Parkinson's disease which was found to aggregate faster and to be more cytotoxic.⁵⁷ We simulated an H50Q mutant of our barrel and found that it remained stable and hydrated for 4 μ s, but then flattened and dried out like the wild type barrel in the remaining 6 μ s (Figure 5). Total β -sheet content diminished from 70 to 55% within 3 μ s and remained stable thereafter.

Because the His has a pK_a of 6.5, it is conceivable that at least some of the His in the interior surface of the barrel might be charged. To examine the effect of this on pore stability, we repeated the above simulation with four of the eight His doubly protonated. In that case the pore also flattened somewhat, but the additional charge attracted enough solvent to keep the pore from collapsing and hydrated for the entire 10 μ s. The flattening is likely caused by hydrophobic interactions and aromatic stacking between the TYR rings. Figure 7 shows the correlation between TYR ring distance, measured between two adjacent strands, and pore diameter, approximated by the distance between two $C_{\alpha}s$ in opposite strands. The total β sheet content dropped from 70% initially to 45% at 1 μ s, and remained stable thereafter (Figure S5). Water molecules that diffuse along the backbones of strands E and F, where the barrel curvature becomes acute, transiently form an intercalating chain at various times (Figure 8). Figure S6 shows the fraction of each lipid type in contact with protein.

DISCUSSION

We have identified two regions of aS that may be able to form at least metastable, oligomeric, membrane-embedded β -barrels: 35–56 and 64–92. The simulations do not prove that the barrels are thermodynamically stable because they start from preformed barrels and have a limited time scale compared to experiment. No account has been taken of the

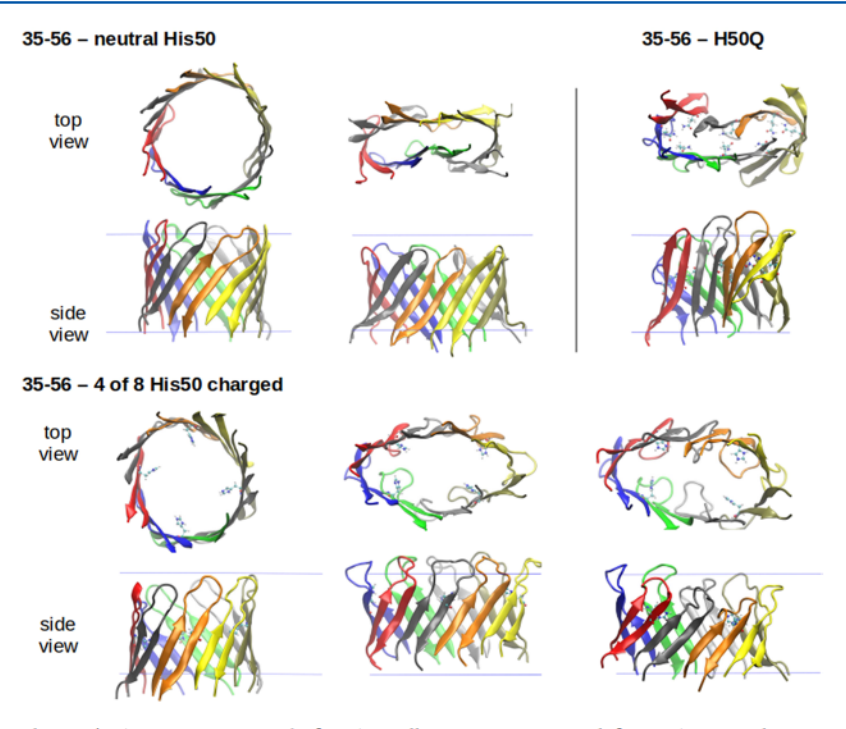


Figure 5. 35–56 oligomer with Y39/H50 pointing inward after 5 μ s all-atom MD. Upper left: His50 neutral at 0 and 5 μ s. Upper right: H50Q mutant at 5 μ s. Lower half: H50 half charged at 0, 5, and 10 μ s.

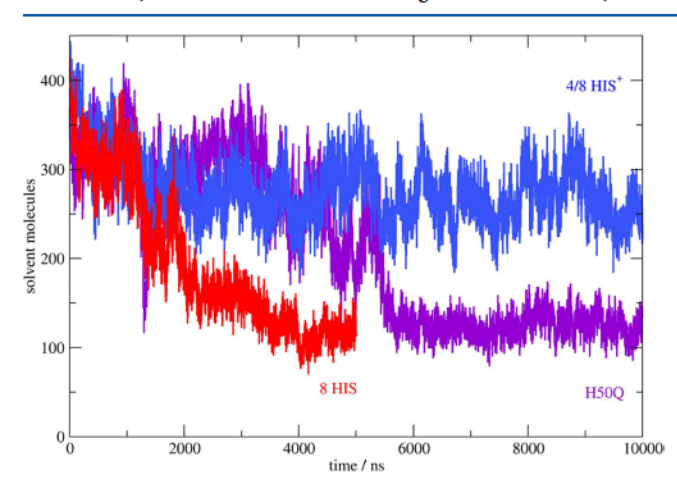


Figure 6. Water molecules inside the $Y_{\rm in}H_{\rm in}$ barrels. Red: Neutral H50. Water drains first from the central hydrophobic TYR area. The molecules that remain reside at the barrel top and bottom, between either the loops or the termini of the hairpins. Blue: Half of the H50 residues are charged. The barrel remains hydrated. Purple: H50Q mutant. Dehydration is delayed.

entropic cost of bringing several hairpins together in a precise register and orientation and no alternative structures were considered. The results only indicate that the structure are plausible and cannot be immediately dismissed. The kinetics of forming these structures, which is also not considered here, is expected to be quite slow but the time scale on which amyloid diseases develop is also very slow. The octameric oligomeric state chosen for our models is nearly the smallest that could allow ion transport. Small variations in aggregation number should not have a large effect on stability. Many aS oligomers have higher aggregation numbers.^{33,58,59} It is possible that not all monomers in an oligomer participate in membrane perturbation.

The hairpins constructed by the NAC fragment give a reasonably stable pore, although a barrel with higher initial shear might have been preferable. For this segment some experimental results on toxic oligomers interacting with membranes are available via solid state NMR.³³ The data showed that residues 70–88 were in β conformation. 70–88 is slightly shorter than our model (64–92) and does not include some strongly hydrophobic residues that stabilize membrane insertion. In NAC5 the residues in β conformation are 67–72 and 86–92, so 70–88 is mostly in the loops. Alignment NAC1 in Table 2 was inspired by these NMR results, but turned out not to be very stable. Perhaps the structure detected in ref 33 is not a barrel; there is no evidence in that work that the oligomers cross the membrane.

What makes fragment 35–56 especially interesting is that the majority of Parkinson's disease familial mutants occur within or near this fragment: A30P, E35K, E46K, H50Q, G51D, and A53T. The biophysical properties of these mutants are well studied: some accelerate aggregation (H50Q $^{60-62}$) while others slow it down (A30P, 63 G51D 62,64). Some reduce binding to and disruption of membranes, some enhance it, and some have no effect. $^{64-69}$ A macrocyclic β -hairpin derived from 35 to 56 was found to be toxic 70 and deletion of the 36–42 fragment prevented toxicity in *C. elegans*. 71 Sequestering 37–54, which was seen to form a hairpin in MD simulations, 72 reduces aggregation and toxicity. 56 These two strands were proposed to form hairpins in oligomers. 22

We found that the 35–56 barrel dehydrates and collapses due to the hydrophobicity of its interior. Although this could result from improper balance of protein—protein and protein—water interactions in the force field used, it seems rather unlikely. The barrel could remain hydrated if some of the His50 are doubly protonated. In neurons the resting intracellular pH is 7.03–7.46⁷³ and it is reported to decrease with age.⁷⁴ Synaptic vesicles have a pH lower by 1.5 units⁷⁵ and during their exocytosis there is strong transient acid-

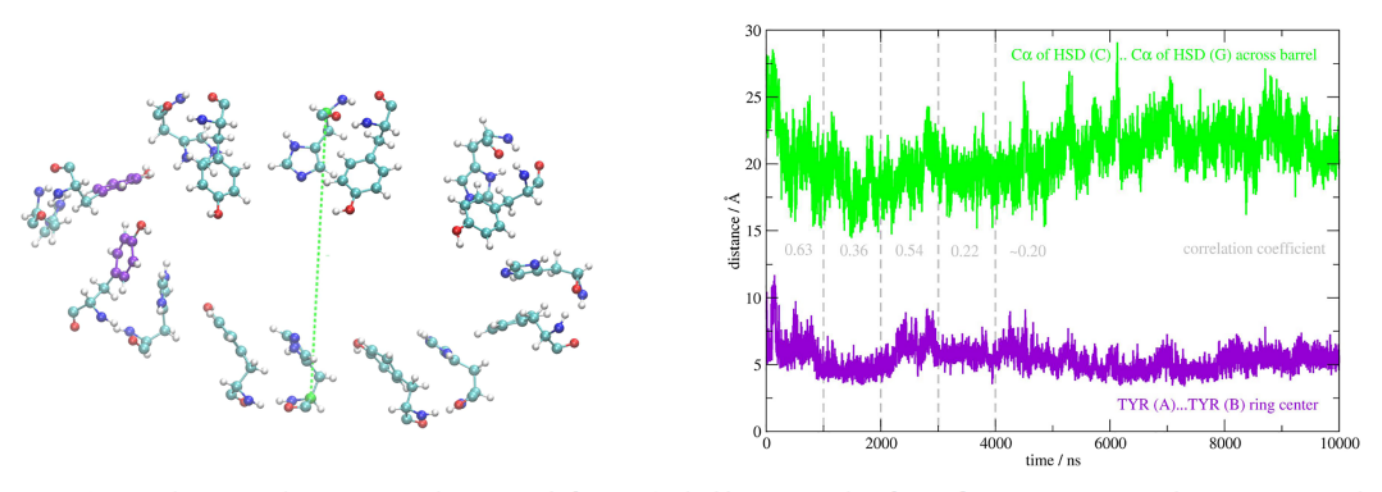


Figure 7. Pore diameter and aromatic ring distances with four His50 doubly protonated. Left: Configuration at 10 μ s. Right: Time series, and correlation coefficients within select trajectory sections between Ca—Ca distance across the barrel and distance between TYR in adjacent strands near one focus of the ellipse.

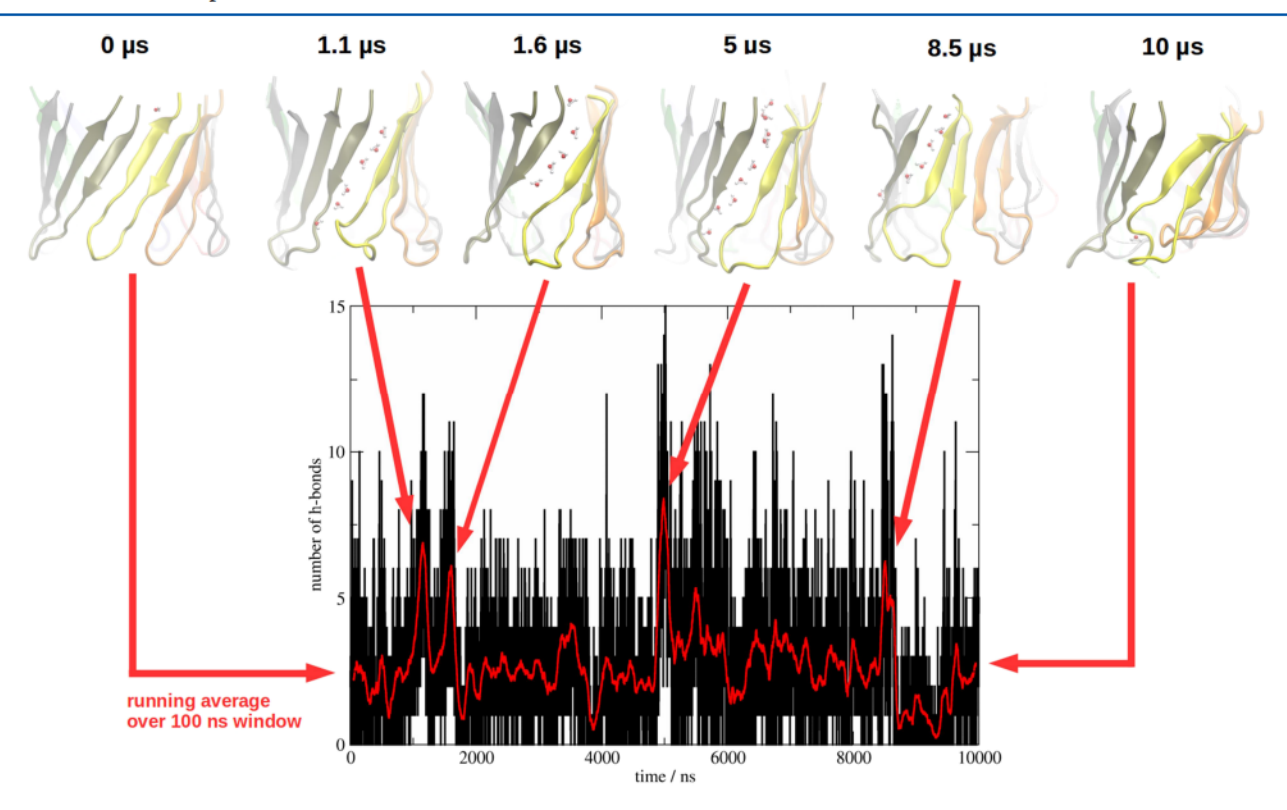


Figure 8. Transient water chain forms at various times in the half-His50-charged 35-56 model. The plot shows the number of H bonds formed by E and F strands with water. A snapshot was taken whenever the running average exceeded 6.

ification of the synaptic cleft.⁷⁶ So, for some periods of time, the pH in some regions may become low enough to protonate His. This finding predicts a pH effect on pore formation by the fragment 35–56, which could be tested by in vitro experiments. A dehydrated barrel could still play a role, for example anchoring the oligomers on the membrane and facilitating their endocytosis from the extracellular medium, a process that has been observed experimentally.⁷⁷

In the $Y_{in}H_{in}$ model that we simulated, G51 is facing lipids, so the mutation G51D would destabilize the pore. The mutant, however, could form a barrel with the C-terminal strand flipped. As shown in Table 3, $Y_{in}H_{out}$ also has favorable insertion energy, albeit less favorable than $Y_{in}H_{in}$. Similarly, A53T/E would stabilize a pore in the flipped conformation,

whereas A53 V would stabilize the pore in the $Y_{in}H_{in}$ strand orientation. The E35K mutation is at the edge of the barrel and the E46K in the loop, surrounded by two other Lysines. The latter might slow down the kinetics of membrane insertion. The substitution of H50 with Q did not help keep the channel open, so the source of the higher extracellular toxicity of this mutant ⁵⁷ should be sought elsewhere, for example in enhanced aggregation.

The presence of H50 within the pore lumen could also mediate some metal effects. His is known to bind Cu, Zn, Fe and other metals.⁷⁸ Inhibition of vesicle leakage by Zn has been observed,⁷⁹ which could be explained by binding of Zn to His in the pore lumen. On the other hand, exposure to metals is a known risk factor for Parkinson's.⁸⁰ Perhaps metals have

two competing effects: first, accelerate oligomerization by tethering together His residues but then inhibit ion leakage by blocking the formed channels.

Experimental structural information on αS oligomers and possible membrane pores is of low-resolution. Early EM and AFM studies of αS and other amyloid-forming proteins showed membrane-bound annular structures $^{35,38,58,81-83}$ with inner diameter of 2–2.5 nm, similar to that of the octamers simulated here. The picture obtained by these studies is likely to be dominated by the extramembranous portions of the protein. We recently applied our methodology to IAPP, amyloid β 1–42, so and amyloid β 25–35 and found reasonably stable β -barrel structures in each case. A recent computational study of a generic FKFE repeat sequence found spontaneous formation of imperfect beta barrels on the time scale of a few μs at somewhat elevated temperatures. These results support the plausibility of the amyloid pore hypothesis.

It may be argued that structures like the ones considered here are too ordered. Indeed, given the high disorder of the oligomers, highly symmetric structures seem unlikely. Perhaps they can be viewed as ideal limits that tell us what is theoretically feasible. It is also possible that oligomers do not form well-defined structures but simply create defects that lower the ion permeation barrier. What actually happens can only be ascertained by careful experimentation. Study of fragments corresponding to our putative membrane-inserting regions would be useful. Lowering the entropy cost of forming these barrels would also facilitate their experimental observation.

METHODS

Implicit Solvent Modeling. Implicit membrane simulations employed the IMM1 model, 90 an extension of the EEF1 effective energy function for soluble proteins 91 to heterogeneous membrane-water systems. IMM1 uses a switching function that transitions smoothly from a nonpolar to an aqueous environment and accounts for the surface potential using the Gouy—Chapman theory. Modeling of pores 93,94 is accomplished by making the switching function F dependent not only on the vertical (z) coordinate but also on the radial coordinate (the distance r from the z axis):

$$F(z', r') = f(z') + b(r') - f(z')b(r'),$$

$$F(z', r') = f(z') + b(r') - f(z')b(r'),$$

$$f(z') = \frac{z'''}{1 + z'''},$$

$$b(r') = 1 - \frac{r'''}{1 + r'''}$$

$$z' = |z|/(T/2), r' = r/R, R = R_o + kz'^2$$
(1)

 β -barrel models of fragments of aS were constructed in two ways. First, by aligning them to the protegrin β -hairpin and using our previously constructed octameric protegrin barrel⁵⁵ as a template. The replaced side chains were built in an extended conformation. Second, we used the NMR structure of a hairpin.⁵⁶ In the latter case the hairpin was first flattened using geometric restraints. Then eight copies were super-

imposed on the template barrel according to backbone RMSD. The structures were refined by a series of energy minimizations and MD simulations in the presence of gradually decreasing H-bonding restraints in an implicit toroidal pore ($R_o = 13$ Å, k = 15 Å). The stability of the barrel was judged by the difference in effective energy of the entire complex in water versus in the membrane pore (transfer energy ΔW), evaluated for the last conformation sampled during the MD simulation in the membrane.

All-Atom Simulations. After the 35–56 barrel with Y39 pointing inside exhibited a favorable ΔW and remained stable over 1.1 ns in the implicit pore, CHARMM GUI was used to place it in an explicit 5:3:2 DOPE:DOPS:DOPC membrane, which is the membrane composition used in recent in vitro experiments.³³ A box size of 100 Å was chosen for the ~40 Å diameter barrel, resulting in 140 lipid molecules. Pore water and KCl counterions were added. The structure was equilibrated in NAMD for 6 ns. After it proved stable for another 9.2 ns, the final structure was submitted to the ANTON 2 supercomputer⁹⁵ and run for 5 μ s. Two protonation states were chosen for the His50 residue, which lines the pore lumen: either all neutral or four of the eight residues doubly protonated. A H50Q mutant was also generated and run for 10 μ s.

The most stable 64–92 model (NAC5) was treated analogously: CHARMM GUI was used to place it in an explicit 5:3:2 DOPE:DOPS:DOPC membrane with a box size of 100 Å. The structure was equilibrated in NAMD for 6 ns. After it proved stable for another 9.7 ns, the final structure was submitted to ANTON 2 and run for 10 μ s. The β -sheet content was calculated using the COOR SECS command in CHARMM, which is based on DSSP.

ASSOCIATED CONTENT

Data Availability Statement

The implicit solvent simulations were carried out with the program CHARMM, which is available by license from Prof. M. Karplus (Harvard University). The all-atom simulations were done with the freely available software NAMD and the Anton software (D.E. Shaw Research), available to grantees at the Pittsburgh Supercomputer Center. The final coordinates of all-atom simulations are provided in Supporting Information. All other structures mentioned in this article are available from the corresponding author upon request. The Anton trajectories are available through the Pittsburgh Supercomputer Center.

Supporting Information

The Supporting Information is available free of charge at https://pubs.acs.org/doi/10.1021/acs.jcim.3c00997.

Figures S1-S6 (PDF)
Final coordinates of the all-atom simulations:
3556_5us (PDB)
3556_h50q_10us (PDB)
3556_hsp_10us (PDB)
6492_10us (PDB)

AUTHOR INFORMATION

Corresponding Author

Themis Lazaridis — Department of Chemistry & Biochemistry, City College of New York/CUNY, New York, New York 10031, United States; orcid.org/0000-0003-4218-7590; Phone: (212) 650-8364; Email: tlazaridis@ccny.cuny.edu

Author

Manuela Maurer — Department of Chemistry & Biochemistry, City College of New York/CUNY, New York, New York 10031, United States; orcid.org/0000-0001-9837-4411

Complete contact information is available at: https://pubs.acs.org/10.1021/acs.jcim.3c00997

Author Contributions

T.L. conceived the project. M.M. performed and analyzed the simulations. M.M. and T.L. wrote the manuscript.

Notes

The authors declare no competing financial interest.

ACKNOWLEDGMENTS

This work was supported by the National Science Foundation (MCB-1855942). Anton computer time was provided by the Pittsburgh Supercomputing Center through grant R01GM116961 from the NIH. The Anton machine at PSC was generously made available by D.E. Shaw Research, and computer time was provided by the National Center for Multiscale Modeling of Biological Systems through grant number P41GM103712-S1 from the NIH and Pittsburgh Supercomputing Center.

REFERENCES

- (1) Goedert, M. Alpha-Synuclein and Neurodegenerative Diseases. *Nat. Rev. Neurosci.* 2001, 2, 492–501.
- (2) Krismer, F.; Wenning, G. K. Multiple System Atrophy: Insights into a Rare and Debilitating Movement Disorder. *Nat. Rev. Neurol.* 2017, 13, 232–243.
- (3) Burré, J. The Synaptic Function of α -Synuclein. J. Parkinsons Dis. 2015, 5, 699–713.
- (4) Sulzer, D.; Edwards, R. H. The Physiological Role of α -Synuclein and Its Relationship to Parkinson's Disease. *J. Neurochem.* 2019, 150, 475–486.
- (5) Eliezer, D.; Kutluay, E.; Bussell, R.; Browne, G. Conformational Properties of α -Synuclein in Its Free and Lipid-Associated States. *J. Mol. Biol.* 2001, 307, 1061–1073.
- (6) Theillet, F. X.; Binolfi, A.; Bekei, B.; Martorana, A.; Rose, H. M.; Stuiver, M.; Verzini, S.; Lorenz, D.; Van Rossum, M.; Goldfarb, D.; Selenko, P. Structural Disorder of Monomeric α -Synuclein Persists in Mammalian Cells. *Nature* 2016, 530, 45–50.
- (7) Chandra, S.; Chen, X.; Rizo, J.; Jahn, R.; Sudhof, T. C. A Broken A-Helix in Folded a-Synuclein. J. Biol. Chem. 2003, 278, 15313—15318.
- (8) Ulmer, T. S.; Bax, A.; Cole, N. B.; Nussbaum, R. L. Structure and Dynamics of Micelle-Bound Human α -Synuclein. *J. Biol. Chem.* 2005, 280, 9595–9603.
- (9) Bortolus, M.; Tombolato, F.; Tessari, I.; Bisaglia, M.; Mammi, S.; Bubacco, L.; Ferrarini, A.; Maniero, A. L. Broken Helix in Vesicle and Micelle-Bound α -Synuclein: Insights from Site-Directed Spin Labeling-EPR Experiments and MD Simulations. *J. Am. Chem. Soc.* 2008, 130, 6690–6691.
- (10) Jao, C. C.; Hegde, B. G.; Chenb, J.; Haworth, I. S.; Langen, R. Structure of Membrane-Bound α -Synuclein from Site-Directed Spin Labeling and Computational Refinement. *Proc. Natl. Acad. Sci. U. S. A.* 2008, 105, 19666–19671.
- (11) Georgieva, E. R.; Ramlall, T. F.; Borbat, P. P.; Freed, J. H.; Eliezer, D. Membrane-Bound Alpha-Synuclein Forms an Extended Helix: Long-Distance Pulsed ESR Measurements Using Vesicles, Bicelles, and Rodlike Micelles. *J. Am. Chem. Soc.* 2008, 130, 12856—12857.
- (12) Trexler, A. J.; Rhoades, E. Alpha-Synuclein Binds Large Unilamellar Vesicles as an Extended Helix. *Biochemistry* 2009, 48, 2304–2306.

- (13) Bekshe Lokappa, S.; Ulmer, T. S. A-Synuclein Populates Both Elongated and Broken Helix States on Small Unilamellar Vesicles. *J. Biol. Chem.* 2011, 286, 21450–21457.
- (14) Tang, M.; Comellas, G.; Rienstra, C. M. Advanced Solid-State NMR Approaches for Structure Determination of Membrane Proteins and Amyloid Fibrils. *Acc. Chem. Res.* 2013, 46, 2080–2088.
- (15) Guerrero-Ferreira, R.; Taylor, N. M. I.; Arteni, A. A.; Kumari, P.; Mona, D.; Ringler, P.; Britschgi, M.; Lauer, M. E.; Makky, A.; Verasdock, J.; Riek, R.; Melki, R.; Meier, B. H.; Böckmann, A.; Bousset, L.; Stahlberg, H. Two New Polymorphic Structures of Human Full-Length Alpha-Synuclein Fibrils Solved by Cryo-Electron Microscopy. *Elife* 2019, 8, No. e48907.
- (16) Boyer, D. R.; Li, B.; Sun, C.; Fan, W.; Zhou, K.; Hughes, M. P.; Sawaya, M. R.; Jiang, L.; Eisenberg, D. S. The α-Synuclein Hereditary Mutation E46K Unlocks a More Stable, Pathogenic Fibril Structure. *Proc. Natl. Acad. Sci. U. S. A.* 2020, 117, 3592–3602.
- (17) Schweighauser, M.; Shi, Y.; Tarutani, A.; Kametani, F.; Murzin, A. G.; Ghetti, B.; Matsubara, T.; Tomita, T.; Ando, T.; Hasegawa, K.; Murayama, S.; Yoshida, M.; Hasegawa, M.; Scheres, S. H. W.; Goedert, M. Structures of α-Synuclein Filaments from Multiple System Atrophy. *Nature* 2020, 585, 464–469.
- (18) Li, B.; Ge, P.; Murray, K. A.; Sheth, P.; Zhang, M.; Nair, G.; Sawaya, M. R.; Shin, W. S.; Boyer, D. R.; Ye, S.; Eisenberg, D. S.; Zhou, Z. H.; Jiang, L. Cryo-EM of Full-Length α-Synuclein Reveals Fibril Polymorphs with a Common Structural Kernel. *Nat. Commun.* 2018, 9, 3609.
- (19) Rodriguez, J. A.; Ivanova, M. I.; Sawaya, M. R.; Cascio, D.; Reyes, F. E.; Shi, D.; Sangwan, S.; Guenther, E. L.; Johnson, L. M.; Zhang, M.; Jiang, L.; Arbing, M. A.; Nannenga, B. L.; Hattne, J.; Whitelegge, J.; Brewster, A. S.; Messerschmidt, M.; Boutet, S.; Sauter, N. K.; Gonen, T.; Eisenberg, D. S. Structure of the Toxic Core of α -Synuclein from Invisible Crystals. *Nature* 2015, 525, 486–490.
- (20) Ingelsson, M. Alpha-Synuclein Oligomers-Neurotoxic Molecules in Parkinson's Disease and Other Lewy Body Disorders. *Front. Neurosci.* 2016, 10, 408.
- (21) Apetri, M. M.; Maiti, N. C.; Zagorski, M. G.; Carey, P. R.; Anderson, V. E. Secondary Structure of α -Synuclein Oligomers: Characterization by Raman and Atomic Force Microscopy. *J. Mol. Biol.* 2006, 355, 63–71.
- (22) Celej, M. S.; Sarroukh, R.; Goormaghtigh, E.; Fidelio, G. D.; Ruysschaert, J. M.; Raussens, V. Toxic Prefibrillar α -Synuclein Amyloid Oligomers Adopt a Distinctive Antiparallel β -Sheet Structure. *Biochem. J.* 2012, 443, 719—726.
- (23) Paslawski, W.; Mysling, S.; Thomsen, K.; Jørgensen, T. J. D.; Otzen, D. E. Co-Existence of Two Different α-Synuclein Oligomers with Different Core Structures Determined by Hydrogen/Deuterium Exchange Mass Spectrometry. *Angew. Chem., Int. Ed.* 2014, 53, 7560–7563.
- (24) Zhou, L.; Kurouski, D. Structural Characterization of Individual α -Synuclein Oligomers Formed at Different Stages of Protein Aggregation by Atomic Force Microscopy-Infrared Spectroscopy. *Anal. Chem.* 2020, 92, 6806–6810.
- (25) Karpinar, D. P.; Balija, M. B. G.; Kügler, S.; Opazo, F.; Rezaei-Ghaleh, N.; Wender, N.; Kim, H. Y.; Taschenberger, G.; Falkenburger, B. H.; Heise, H.; Kumar, A.; Riedel, D.; Fichtner, L.; Voigt, A.; Braus, G. H.; Giller, K.; Becker, S.; Herzig, A.; Baldus, M.; Jäckle, H.; Eimer, S.; Schulz, J. B.; Griesinger, C.; Zweckstetter, M. Pre-Fibrillar α -Synuclein Variants with Impaired B-Structure Increase Neurotoxicity in Parkinson's Disease Models. *EMBO J.* 2009, 28, 3256–3268.
- (26) Winner, B.; Jappelli, R.; Maji, S. K.; Desplats, P. A.; Boyer, L.; Aigner, S.; Hetzer, C.; Loher, T.; Vilar, M.; Campioni, S.; Tzitzilonis, C.; Soragni, A.; Jessberger, S.; Mira, H.; Consiglio, A.; Pham, E.; Masliah, E.; Gage, F. H.; Riek, R. In Vivo Demonstration That α -Synuclein Oligomers Are Toxic. *Proc. Natl. Acad. Sci. U. S. A.* 2011, 108, 4194–4199.
- (27) Pieri, L.; Madiona, K.; Bousset, L.; Melki, R. Fibrillar α -Synuclein and Huntingtin Exon 1 Assemblies Are Toxic to the Cells. *Biophys. J.* 2012, *102*, 2894–2905.

- (28) Peelaerts, W.; Bousset, L.; Van Der Perren, A.; Moskalyuk, A.; Pulizzi, R.; Giugliano, M.; Van Den Haute, C.; Melki, R.; Baekelandt, V. α -Synuclein Strains Cause Distinct Synucleinopathies after Local and Systemic Administration. *Nature* 2015, 522, 340–344.
- (29) Bengoa-Vergniory, N.; Roberts, R. F.; Wade-Martins, R.; Alegre-Abarrategui, J. Alpha-Synuclein Oligomers: A New Hope. *Acta Neuropathol.* 2017, 134, 819—838.
- (30) Volles, M. J.; Lee, S. J.; Rochet, J. C.; Shtilerman, M. D.; Ding, T. T.; Kessler, J. C.; Lansbury, P. T. Vesicle Permeabilization by Protofibrillar α -Synuclein: Implications for the Pathogenesis and Treatment of Parkinson's Disease. *Biochemistry* 2001, 40, 7812–7819.
- (31) Lorenzen, N.; Nielsen, S. B.; Buell, A. K.; Kaspersen, J. D.; Arosio, P.; Vad, B. S.; Paslawski, W.; Christiansen, G.; Valnickova-Hansen, Z.; Andreasen, M.; Enghild, J. J.; Pedersen, J. S.; Dobson, C. M.; Knowles, T. P. J.; Otzen, D. E. The Role of Stable α-Synuclein Oligomers in the Molecular Events Underlying Amyloid Formation. J. Am. Chem. Soc. 2014, 136, 3859–3868.
- (32) Ghio, S.; Camilleri, A.; Caruana, M.; Ruf, V. C.; Schmidt, F.; Leonov, A.; Ryazanov, S.; Griesinger, C.; Cauchi, R. J.; Kamp, F.; Giese, A.; Vassallo, N. Cardiolipin Promotes Pore-Forming Activity of Alpha-Synuclein Oligomers in Mitochondrial Membranes. *ACS Chem. Neurosci.* 2019, 10, 3815–3829.
- (33) Fusco, G.; Chen, S. W.; Williamson, P. T. F.; Cascella, R.; Perni, M.; Jarvis, J. A.; Cecchi, C.; Vendruscolo, M.; Chiti, F.; Cremades, N.; Ying, L.; Dobson, C. M.; De Simone, A. Structural Basis of Membrane Disruption and Cellular Toxicity by A-Synuclein Oligomers. *Science* 2017, 358, 1440–1443.
- (34) Volles, M. J.; Lansbury, P. T., Jr Zeroing in on the Pathogenic Form of Alpha-Synuclein and Its Mechanism of Neurotoxicity in Parkinson's Disease. *Biochemistry* 2003, 42, 7871–7878.
- (35) Quist, A.; Doudevski, I.; Lin, H.; Azimova, R.; Ng, D.; Frangione, B.; Kagan, B.; Ghiso, J.; Lal, R. Amyloid Ion Channels: A Common Structural Link for Protein-Misfolding Disease. *Proc. Natl. Acad. Sci. U. S. A.* 2005, 102, 10427–10432.
- (36) Furukawa, K.; Matsuzaki-Kobayashi, M.; Hasegawa, T.; Kikuchi, A.; Sugeno, N.; Itoyama, Y.; Wang, Y.; Yao, P. J.; Bushlin, I.; Takeda, A. Plasma Membrane Ion Permeability Induced by Mutant α -Synuclein Contributes to the Degeneration of Neural Cells. *J. Neurochem.* 2006, 97, 1071–1077.
- (37) Zakharov, S. D.; Hulleman, J. D.; Dutseva, E. A.; Antonenko, Y. N.; Rochet, J. C.; Cramer, W. A. Helical α-Synuclein Forms Highly Conductive Ion Channels. *Biochemistry* 2007, 46, 14369–14379.
- (38) Danzer, K. M.; Haasen, D.; Karow, A. R.; Moussaud, S.; Habeck, M.; Giese, A.; Kretzschmar, H.; Hengerer, B.; Kostka, M. Different Species of α -Synuclein Oligomers Induce Calcium Influx and Seeding. *J. Neurosci.* 2007, 27, 9220–9232.
- (39) Kim, H. Y.; Cho, M. K.; Kumar, A.; Maier, E.; Siebenhaar, C.; Becker, S.; Fernandez, C. O.; Lashuel, H. A.; Benz, R.; Lange, A.; Zweckstetter, M. Structural Properties of Pore-Forming Oligomers of Alpha-Synuclein. *J. Am. Chem. Soc.* 2009, 131, 17482–17489.
- (40) van Rooijen, B. D.; Claessens, M. M. A. E.; Subramaniam, V. Lipid Bilayer Disruption by Oligomeric α-Synuclein Depends on Bilayer Charge and Accessibility of the Hydrophobic Core. *Biochim. Biophys. Acta, Biomembr.* 2009, 1788, 1271–1278.
- (41) Tosatto, L.; Andrighetti, A. O.; Plotegher, N.; Antonini, V.; Tessari, I.; Ricci, L.; Bubacco, L.; Dalla Serra, M. Alpha-Synuclein Pore Forming Activity upon Membrane Association. *Biochim. Biophys. Acta, Biomembr.* 2012, 1818, 2876–2883.
- (42) Van Maarschalkerweerd, A.; Vetri, V.; Langkilde, A. E.; Foderà, V.; Vestergaard, B. Protein/Lipid Coaggregates Are Formed during α -Synuclein-Induced Disruption of Lipid Bilayers. *Biomacromolecules* 2014, 15, 3643–3654.
- (43) Hannestad, J. K.; Rocha, S.; Agnarsson, B.; Zhdanov, V. P.; Zhdanov, V. P.; Wittung-Stafshede, P.; Höök, F. Single-Vesicle Imaging Reveals Lipid-Selective and Stepwise Membrane Disruption by Monomeric a-Synuclein. *Proc. Natl. Acad. Sci. U. S. A.* 2020, 117, 14178—14186.

- (44) Nguyen, P. H.; Derreumaux, P. Structures of the Intrinsically Disordered $A\beta$, Tau and α -Synuclein Proteins in Aqueous Solution from Computer Simulations. *Biophys. Chem.* 2020, 264, No. 106421.
- (45) Vermaas, J. V.; Tajkhorshid, E. Conformational Heterogeneity of α-Synuclein in Membrane. *Biochim. Biophys. Acta, Biomembr.* 2014, 1838, 3107–3117.
- (46) West, A.; Brummel, B. E.; Braun, A. R.; Rhoades, E.; Sachs, J. N. Membrane Remodeling and Mechanics: Experiments and Simulations of α -Synuclein. *Biochim. Biophys. Acta, Biomembr.* **2016**, 1858, 1594–1609.
- (47) Kang, C.; Sun, R. Molecular Dynamics Study of the Interaction between the N-Terminal of α -Synuclein and a Lipid Bilayer Mimicking Synaptic Vesicles. *J. Phys. Chem. B* **2021**, *125*, 1036–1048.
- (48) Tsigelny, I. F.; Sharikov, Y.; Wrasidlo, W.; Gonzalez, T.; Desplats, P. A.; Crews, L.; Spencer, B.; Masliah, E. Role of α -Synuclein Penetration into the Membrane in the Mechanisms of Oligomer Pore Formation. *FEBS J.* 2012, 279, 1000–1013.
- (49) Tsigelny, I. F.; Sharikov, Y.; Kouznetsova, V. L.; Greenberg, J. P.; Wrasidlo, W.; Overk, C.; Gonzalez, T.; Trejo, M.; Spencer, B.; Kosberg, K.; Masliah, E. Molecular Determinants of α -Synuclein Mutants' Oligomerization and Membrane Interactions. *ACS Chem. Neurosci.* 2015, 6, 403–416.
- (50) Durell, S. R.; Guy, H. R. The Amyloid Concentric β-Barrel Hypothesis: Models of Synuclein Oligomers, Annular Protofibrils, Lipoproteins, and Transmembrane Channels. *Proteins: Struct. Funct. Bioinf.* 2022, 90, 512–542.
- (51) Mihajlovic, M.; Lazaridis, T. Membrane-Bound Structure and Energetics of Alpha-Synuclein. *Proteins: Struct. Funct. Bioinf.* 2008, 70, 761–778.
- (52) Nepal, B.; Leveritt, J.; Lazaridis, T. Membrane Curvature Sensing by Amphipathic Helices: Insights from Implicit Membrane Modeling. *Biophys. J.* 2018, 114, 2128–2141.
- (53) Wimley, W. C. Toward Genomic Identification of Beta-Barrel Membrane Proteins: Composition and Architecture of Known Structures. *Protein Sci.* 2002, 11, 301–312.
- (54) Dhar, R.; Feehan, R.; Slusky, J. S. G. Membrane Barrels Are Taller, Fatter, Inside-Out Soluble Barrels. *J. Phys. Chem. B* 2021, 125, 3622–3628.
- (55) Lipkin, R.; Pino-Angeles, A.; Lazaridis, T. Transmembrane Pore Structures of β -Hairpin Antimicrobial Peptides by All-Atom Simulations. *J. Phys. Chem. B* **2017**, *121*, 9126–9140.
- (56) Mirecka, E. A.; Shaykhalishahi, H.; Gauhar, A.; Akgül, Ş.; Lecher, J.; Willbold, D.; Stoldt, M.; Hoyer, W. Sequestration of a β -Hairpin for Control of α -Synuclein Aggregation. *Angew. Chem., Int. Ed.* 2014, 53, 4227–4230.
- (57) Khalaf, O.; Fauvet, B.; Oueslati, A.; Dikiy, I.; Mahul-Mellier, A. L.; Ruggeri, F. S.; Mbefo, M. K.; Vercruysse, F.; Dietler, G.; Lee, S. J.; Eliezer, D.; Lashuel, H. A. The H50Q Mutation Enhances $A\alpha$ -Synuclein Aggregation, Secretion, and Toxicity. *J. Biol. Chem.* 2014, 289, 21856—21876.
- (58) Lashuel, H. A.; Hartley, D.; Petre, B. M.; Walz, T.; Lansbury, P. T. Neurodegenerative Disease: Amyloid Pores from Pathogenic Mutations. *Nature* 2002, 418, 291.
- (59) Zijlstra, N.; Blum, C.; Segers-Nolten, I. M. J.; Claessens, M. M. A. E.; Subramaniam, V. Molecular Composition of Sub-Stoichiometrically Labeled α -Synuclein Oligomers Determined by Single-Molecule Photobleaching. *Angew. Chem., Int. Ed.* 2012, 51, 8821–8824.
- (60) Ghosh, D.; Mondal, M.; Mohite, G. M.; Singh, P. K.; Ranjan, P.; Anoop, A.; Ghosh, S.; Jha, N. N.; Kumar, A.; Maji, S. K. The Parkinson's Disease-Associated H50Q Mutation Accelerates α -Synuclein Aggregation in Vitro. *Biochemistry* 2013, 52, 6925–6927.
- (61) Chi, Y. C.; Armstrong, G. S.; Jones, D. N. M.; Eisenmesser, E. Z.; Liu, C. W. Residue Histidine 50 Plays a Key Role in Protecting α -Synuclein from Aggregation at Physiological PH. *J. Biol. Chem.* 2014, 289, 15474—15481.
- (62) Rutherford, N. J.; Moore, B. D.; Golde, T. E.; Giasson, B. I. Divergent Effects of the H50Q and G51D SNCA Mutations on the Aggregation of α -Synuclein. *J. Neurochem.* 2014, 131, 859–867.

- (63) Conway, K. A.; Lee, S. J.; Rochet, J. C.; Ding, T. T.; Williamson, R. E.; Lansbury, P. T. Acceleration of Oligomerization, Not Fibrillization, Is a Shared Property of Both α -Synuclein Mutations Linked to Early-Onset Parkinson's Disease: Implications for Pathogenesis and Therapy. *Proc. Natl. Acad. Sci. U. S. A.* 2000, 97, 571–576.
- (64) Fares, M. B.; Ait-Bouziad, N.; Dikiy, I.; Mbefo, M. K.; Jovičić, A.; Kiely, A.; Holton, J. L.; Lee, S. J.; Gitler, A. D.; Eliezer, D.; Lashuel, H. A. The Novel Parkinson's Disease Linked Mutation G51D Attenuates in Vitro Aggregation and Membrane Binding of α -Synuclein, and Enhances Its Secretion and Nuclear Localization in Cells. *Hum. Mol. Genet.* 2014, 23, 4491–4509.
- (65) Jensen, P. H.; Nielsen, M. S.; Jakes, R.; Dotti, C. G.; Goedert, M. Binding of α -Synuclein to Brain Vesicles Is Abolished by Familial Parkinson's Disease Mutation. *J. Biol. Chem.* 1998, 273, 26292–26294.
- (66) Jo, E.; Fuller, N.; Rand, R. P.; St George-Hyslop, P.; Fraser, P. E. Defective Membrane Interactions of Familial Parkinson's Disease Mutant A30P α -Synuclein. *J. Mol. Biol.* 2002, 315, 799–807.
- (67) Bussell, R.; Eliezer, D. Effects of Parkinson's Disease-Linked Mutations on the Structure of Lipid-Associated Alpha-Synuclein. *Biochemistry* 2004, 43, 4810–4818.
- (68) Kim, Y. S.; Laurine, E.; Woods, W.; Lee, S. J. A Novel Mechanism of Interaction between α-Synuclein and Biological Membranes. *J. Mol. Biol.* **2006**, *360*, *386*–397.
- (69) Stefanovic, A. N. D.; Lindhoud, S.; Semerdzhiev, S. A.; Claessens, M. M. A. E.; Subramaniam, V. Oligomers of Parkinson's Disease-Related α -Synuclein Mutants Have Similar Structures but Distinctive Membrane Permeabilization Properties. *Biochemistry* 2015, 54, 3142–3150.
- (70) Salveson, P. J.; Spencer, R. K.; Nowick, J. S. X-Ray Crystallographic Structure of Oligomers Formed by a Toxic β -Hairpin Derived from α -Synuclein: Trimers and Higher-Order Oligomers. J. Am. Chem. Soc. 2016, 138, 4458–4467.
- (71) Doherty, C. P. A.; Ulamec, S. M.; Maya-Martinez, R.; Good, S. C.; Makepeace, J.; Khan, G. N.; van Oosten-Hawle, P.; Radford, S. E.; Brockwell, D. J. A Short Motif in the N-Terminal Region of α -Synuclein Is Critical for Both Aggregation and Function. *Nat. Struct. Mol. Biol.* 2020, 27, 249–259.
- (72) Yu, H.; Han, W.; Ma, W.; Schulten, K. Transient β -Hairpin Formation in α -Synuclein Monomer Revealed by Coarse-Grained Molecular Dynamics Simulation. *J. Chem. Phys.* 2015, 143, 243142.
- (73) Ruffin, V. A.; Salameh, A. I.; Boron, W. F.; Parker, M. D. Intracellular PH Regulation by Acid-Base Transporters in Mammalian Neurons. *Front. Physiol.* **2014**, *5*, 43.
- (74) Bonnet, U.; Bingmann, D.; Speckmann, E. J.; Wiemann, M. Aging Is Associated with a Mild Acidification in Neocortical Human Neurons in Vitro. *J. Neural Transm.* 2018, 125, 1495–1501.
- (75) DeVries, S. H. Exocytosed Protons Feedback to Suppress the Ca2+ Current in Mammalian Cone Photoreceptors. *Neuron* 2001, 32, 1107–1117.
- (76) Sinning, A.; Hübner, C. A. Minireview: PH and Synaptic Transmission. FEBS Lett. 2013, 587, 1923–1928.
- (77) Morten, M. J.; Sirvio, L.; Rupawala, H.; Hayes, E. M.; Franco, A.; Radulescu, C.; Ying, L.; Barnes, S. J.; Muga, A.; Ye, Y. Quantitative Super-Resolution Imaging of Pathological Aggregates Reveals Distinct Toxicity Profiles in Different Synucleinopathies. *Proc. Natl. Acad. Sci. U. S. A.* 2022, 119, No. e2205591119.
- (78) González, N.; Arcos-López, T.; König, A.; Quintanar, L.; Menacho Márquez, M.; Outeiro, T. F.; Fernández, C. O. Effects of Alpha-Synuclein Post-Translational Modifications on Metal Binding. *J. Neurochem.* 2019, 150, 507–521.
- (79) Caruana, M.; Neuner, J.; Högen, T.; Schmidt, F.; Kamp, F.; Scerri, C.; Giese, A.; Vassallo, N. Polyphenolic Compounds Are Novel Protective Agents against Lipid Membrane Damage by α-Synuclein Aggregates in Vitro. *Biochim. Biophys. Acta, Biomembr.* 2012, 1818, 2502–2510.
- (80) Uversky, V. N.; Li, J.; Fink, A. L. Metal-Triggered Structural Transformations, Aggregation, and Fibrillation of Human α -

- Synuclein: A Possible Molecular Link between Parkinson's Disease and Heavy Metal Exposure. J. Biol. Chem. 2001, 276, 44284–44296.
- (81) Lashuel, H. A.; Petre, B. M.; Wall, J.; Simon, M.; Nowak, R. J.; Walz, T.; Lansbury, P. T. A-Synuclein, Especially the Parkinson'S Disease-Associated Mutants, Forms Pore-Like Annular and Tubular Protofibrils. *J. Mol. Biol.* 2002, 322, 1089–1102.
- (82) Ding, T. T.; Lee, S. J.; Rochet, J. C.; Lansbury, P. T. Annular α -Synuclein Protofibrils Are Produced When Spherical Protofibrils Are Incubated in Solution or Bound to Brain-Derived Membranes. *Biochemistry* 2002, 41, 10209–10217.
- (83) Lashuel, H. A.; Lansbury, P. T. Are Amyloid Diseases Caused by Protein Aggregates That Mimic Bacterial Pore-Forming Toxins? *Q. Rev. Biophys.* 2006, 39, 167–201.
- (84) Sepehri, A.; Nepal, B.; Lazaridis, T. Distinct Modes of Action of IAPP Oligomers on Membranes. J. Chem. Inf. Model. 2021, 61, 4645–4655
- (85) Sepehri, A.; Lazaridis, T. Putative Structures of Membrane-Embedded Amyloid β Oligomers. ACS Chem. Neurosci. 2023, 14, 99–110.
- (86) Dutta, A.; Sepehri, A.; Lazaridis, T. Putative Pore Structures of Amyloid β 25–35 in Lipid Bilayers. *Biochemistry* 2023, 62, 2549–2558.
- (87) Yang, Y.; Distaffen, H.; Jalali, S.; Nieuwkoop, A. J.; Nilsson, B. L.; Dias, C. L. Atomic Insights into Amyloid-Induced Membrane Damage. ACS Chem. Neurosci. 2022, 13, 2766–2777.
- (88) Stöckl, M. T.; Zijlstra, N.; Subramaniam, V. α-Synuclein Oligomers: An Amyloid Pore? Insights into Mechanisms of α-Synuclein Oligomer-Lipid Interactions. *Mol. Neurobiol.* 2013, 47, 613–621.
- (89) Wu, J.; Blum, T. B.; Farrell, D. P.; DiMaio, F.; Abrahams, J. P.; Luo, J. Cryo-Electron Microscopy Imaging of Alzheimer's Amyloid-Beta 42 Oligomer Displayed on a Functionally and Structurally Relevant Scaffold. *Angew. Chem., Int. Ed.* 2021, 60, 18680–18687.
- (90) Lazaridis, T. Effective Energy Function for Proteins in Lipid Membranes. *Proteins: Struct. Funct. Bioinf.* 2003, 52, 176–192.
- (91) Lazaridis, T.; Karplus, M. Effective Energy Function for Proteins in Solution. *Proteins: Struct. Funct. Bioinf.* 1999, 35, 133–152.
- (92) Lazaridis, T. Implicit Solvent Simulations of Peptide Interactions with Anionic Lipid Membranes. *Proteins: Struct. Funct. Bioinf.* 2005, 58, 518–527.
- (93) Mihajlovic, M.; Lazaridis, T. Antimicrobial Peptides Bind More Strongly to Membrane Pores. *Biochim. Biophys. Acta, Biomembr.* 2010, 1798, 1494–1502.
- (94) Lazaridis, T. Structural Determinants of Transmembrane Beta-Barrels. J. Chem. Theory Comput. 2005, 1, 716–722.
- (95) Shaw, D. E.; Grossman, J. P.; Bank, J. A.; Batson, B.; Butts, J. A.; Chao, J. C.; Deneroff, M. M.; Dror, R. O.; Even, A.; Fenton, C. H.; Forte, A.; Gagliardo, J.; Gill, G.; Greskamp, B.; Ho, C. R.; Ierardi, D. J.; Iserovich, L.; Kuskin, J. S.; Larson, R. H.; Layman, T.; Lee, L. S.; Lerer, A. K.; Li, C.; Killebrew, D.; Mackenzie, K. M.; Mok, S. Y. H.; Moraes, M. A.; Mueller, R.; Nociolo, L. J.; Peticolas, J. L.; Quan, T.; Ramot, D.; Salmon, J. K.; Scarpazza, D. P.; Ben Schafer, U.; Siddique, N.; Snyder, C. W.; Spengler, J.; Tang, P. T. P.; Theobald, M.; Toma, H.; Towles, B.; Vitale, B.; Wang, S. C.; Young, C. Anton 2: Raising the Bar for Performance and Programmability in a Special-Purpose Molecular Dynamics Supercomputer. Int. Conf. High Perform. Comput. Networking, Storage Anal. SC 2014, 41–53.
- (96) Kabsch, W.; Sander, C. Dictionary of Protein Secondary Structure: Pattern Recognition of Hydrogen-bonded and Geometrical Features. *Biopolymers* 1983, 22, 2577–2637.